International Journal of Design & Nature and Ecodynamics
Vol. 19, No. 4, August, 2024, pp. 1317-1325
Journal homepage: http://iieta.org/journals/ijdne

Comprehensive Characterization of Karst Depressions in the Northwestern Yucatan Peninsula Using LiDAR and ASTER GDEM Data

José Francisco Rodríguez-Castillo[1], Oscar Frausto-Martínez[2*]

[1] Master of Science in Marine and Coastal Sciences, Autonomous University of the State of Quintana Roo, City of Cozumel 77600, Mexico
[2] Space Observation and Research Laboratory, Autonomous University of the State of Quintana Roo, City of Cozumel 77600, Mexico

Corresponding Author Email: ofrausto@uqroo.edu.mx

https://doi.org/10.18280/ijdne.190424

Received: 1 April 2024
Revised: 4 June 2024
Accepted: 22 June 2024
Available online: 28 August 2024

Keywords:
coupled models, remote sensing, sinkholes, geomorphology, GIS

ABSTRACT

The present study aims to analyze and classify karst depressions in the northeastern coastal region of the Yucatan Peninsula. The karst relief was analyzed from two data sources: a) a mosaic of LiDAR (light detection and ranging) data, and b) a mosaic of AsterGDEM (Advanced Spaceborne Thermal Emission and Reflection Radiometer Global Digital Elevation Model) data, which were coupled to generate altimetric data and base models. Subsequently, contour lines were generated by differentiating depressions with a minimum depth of 1m; processing and classifying the depressions by applying an analysis of morphometric measurements, morphological profile classification ("V," "U" and "box") and elongation index (sinkholes, sinkholes-uvulas, uvulas, and poljes). A total of 10672 depressions were identified, where 67% correspond to V-type depressions, 23% to U-type, and 10% to box-type; regarding the elongation index, 18% are sinkholes, 42% sinkholes-uvalas, 13% uvalas, and 27% poljes, being the uvalas and poljes the most complex, due to the structural control of the Holbox and Tikul fault system, with a primary orientation of NE7°SW and secondary orientation of SE83°NW. In addition, an inventory of karst depressions is presented, serving as a basis for managing the coastal karst territory at the municipal level.

1. INTRODUCTION

The study of morphological relief allows the proper classification of karst forms, elements, and structures, which helps to determine the genesis, evolution, and geomorphological dynamics. Implementing tools with new methods and technologies helps to develop more accurate studies in areas with low altitudinal contrast. Karst geomorphology studies feature on the surface of soluble rocks by dissolution or related processes [1, 2].

The study of karst relief allows us to understand the genesis of the forms and the dynamics of current landscapes, in addition to providing traces of the paleogeography of the planet [3-5]. This is because the effect of karstification reconfigures the relief of the territory, which, together with the lack of consideration for groundwater with the disorderly growth of urban areas, impermeabilizes the soil [6, 7]. The relief analysis of low altitude contrast and areas of dense vegetation cover presents challenges that, with new technologies and adapted methodologies, allow better reliability and quantity of data to generate indices and fine-scale morphometric analysis [8].

Detailed characterizations contribute to the study of karst in areas of low-relief contrast and are a window into the Yucatan Peninsula's knowledge [9]. Karst is a term for modeling the earth's surface when limestone or other soluble rocks are dominant [10]. Karst zones are natural expressions of karst, with characteristic features on the surface (exokarst) and in the subsoil (endokarst) [11, 12].

These karstification phenomena reconfigure the territory, which must be considered in all land-use planning to preserve and conserve it [7]. Anthropogenic activity impacts both the surface karst and the underground cave system, which are subjected to mechanical destruction with an equal increase in chemical impact because of the input of contaminated runoff moving through increasingly deeper horizons in the soil [13-15].

The combination of a range of systematic geophysical mapping techniques is the practical methodology for modeling the coastal karst landscape; LiDAR technology, microgravity analysis, and standard field mapping methods are procedures that facilitate long-term resource monitoring, which is crucial to karst resource management [16].

Siart et al. [17] examined the application and quality of SRTM and ASTER DEM digital elevation models and GIS techniques for the detection and mapping of karst landforms (mainly closed depressions) at different scales in the Ida Mountains of central Crete, showing that neither of the two models can detect small-scale karst depressions (doline, sinkhole or uvala is a closed depression that drains

underground in karst areas. It can be cylindrical, conical, bowl or plate-shaped. The diameter varies from a few to many hundreds of meters). However, for the recognition of karst depressions with LiDAR, visual recognition and manual digitization are facilitated by the high resolution of the digital elevation model; however, this process becomes tedious due to the large number of sinkholes encountered, derived from the high-resolution density of the model [18]. The heterogeneous karstic relief has different morphometric variables in its depressions, as demonstrated by Fragoso-Servón et al. [10] and Paredes et al. [19], in the Yucatán peninsula, using models with a minimum resolution of 15m and 1:50 000 scale hypsometric contour lines, this spatial resolution was a limiting factor in their approximations.

This study combines two data sources. First, using LiDAR for topographic surveys provides altimetry information from areas of low altitude contrast and high vegetation cover [20, 21]. However, these data are not available for the entire study territory, so a second data source was used, the ASTER GDEM (Advanced Spaceborne Thermal Emission and Reflection Radiometer Global Digital Elevation Model), which has altimetric information for the entire earth's surface, by correlating individual stereoscopic images, helping to add to the altimetric information. This leads to the creation of digital elevation models (DEM) to provide analysis inputs without topographic information [8, 9, 21-24].

Karst relief can be studied through 3D monitoring and the generation of DEMs. These models originate from extracting altimetric data from DTMs or digitizing contour lines and interpolating altitudinal data using Geographic Information Systems (GIS) tools [8].

2. BACKGROUND

Analytical approaches have focused mainly on producing precise information about the relief forms in the karstic soil of the Yucatan Peninsula, which has historically been over-generalized in official geographic-cartographic information [25, 26]. Lindsey et al. [27] analyzed the relationship between karst depression density and anthropogenic activities in the eastern United States, generating four density categories: a) high (>25 depressions/100km^2), b) medium (1-25 depressions/100km^2) and c) low (<1 depression/100km^2), and used water quality as an indicator of the impact of anthropogenic activity, with the variables of pesticide concentration and percentage of CO_2, examining the relationship utilizing non-parametric statistical tests.

Studies such as the one by Fragoso-Servón et al. [10], applying the compactness index emphasizes the methods and algorithms for classifying karst depressions by differentiating the units into three main categories: poljes, uvalas, and sinkholes. This laid the groundwork for Fragoso-Servón et al. [28], who analyzed the karstic processes and the presence of faults using Landsat 7 ETM images from 2010 and 1:50,000 scale cartography through a geomorphopedological approach.

The information generated in studies of karst relief is of importance for risk prevention, as demonstrated by the work of Pereira-Corona et al. [29], in which superimposing layers of data from the 2013 digital terrain model (DTM) and 1:250 000 and 1:50 000 scale cartography, he demonstrated the importance of studies of edaphology, geology, geomorphology, and hydrology, employing a flood risk map at the Quintana Roo level.

Subsequently, Fuchs et al. [23] analyzed the topographic profile using vectorial software and a DTM, in which they traced the topographic cut they used to draw the relief. Along the same topographic profile line, Ferreira and Uagoda [30] analyzed the topographic form of the depressions, where information from previous studies had been collected, and classified sinkholes in whose typology 3 elements stood out due to the type of profile (cauldron, directed and cenote).

One of the first approaches in the recognition of semi-automated or automated analysis of karst relief with the use of LiDAR was made by Rahimi and Alexander [31], in which employing four stages automated the recognition of erosive zones associated with karst depressions, in stage one were located the local minimum points, in stage one the local minimum points were located, in which the model is processed as a matrix, in which each cell represents the height value and, using the kernel windows, the zones of pixels of lower height are linked and delimited, in the second stage the contours of the depressions around each point are delineated, the third stage concentrates on the characterization; the final stage is based on the purification of false positives, thus managing to find 127 depressions of which 97 real ones, however, this methodology discards sinkholes of small morphometric value (with a small area or large shallow ones). In the same year, Miao et al. [32] made a comparison of three automatic detection methods; the first one analyzed was flood simulation, which uses the cumulative height increments of the catchment to delineate the relief depressions; however, this method proved to be too time-consuming, and also to improve its accuracy it requires more detail because it processes each karst depression individually, the second method was erosion reconstruction (a method used by Rahimi and Alexander [31]) in which he found that the drawback of this standard mythological operator is that the derived depths are overestimated. The third method segments the study area by comparing the morphometric values and then intercepts the detailed count with the ridge lines.

Frausto-Martinez et al. [20] used new technologies from geographic information system methodologies and tools to produce generated inputs with a data resolution of 5 m for the X and Y axes and 15-20 cm for the Z axis. This identified karst depressions and led to new exokarstic cartography with low-altitude contrast. This methodology and inputs allowed analyses such as those by Colín-Olivares et al. [22], which used the DEM obtained from LiDAR data to perform 2 comparative procedures to obtain the relative depth (direct relationship between the highest and lowest levels) of the karst depressions, using a method for raster data and one for vector data. Later, Frausto-Martínez et al. [8] used topographic profiles semi-automatically to classify three types of depression shapes: “V”, “U” and “bowl”. Finally, Frausto-Martínez et al. [20] presented a classification by elongation index, using the major and minor axes, giving four classifications: sinkholes, sinkholes-uvalas, uvalas, and poljes.

Lei et al. [33] implement sonar technologies using special algorithms and image fusion to locate karst caves. This locates the units within a designated time domain, improving efficiency in cave discovery. Thus, it evidences the importance of new advanced detection methods for studying karst relief.

The study presented by Fuchs et al. [23] introduced a semi-automated mapping approach that allows for the spatial analysis of possible depressions through a geomorphometric approach using digital elevation models. This evidence the crucial importance of having a complete inventory of

depressions to assess the karst landscape's susceptibility to change accurately.

Telbisz et al. [21] show the advantage of using digital LiDAR models for the geomorphological characterization of small-scale karst depressions and the modeling of their size distribution through morphometric parameters, which helps to explain the features.

3. MATERIALS AND METHODS

3.1 Study area

The town of Solidaridad is in the northeast of the Yucatan Peninsula-Mexico, from the Playa del Carmen region on the northeast coast inland with Coba to the southwest [24] (Figure 1). It is made up of limestone rock that contains large dissolution conduits, which gives it a karstic landscape that means the aquifer is highly vulnerable to contamination due to the infiltration of contaminated water, saline intrusion, discharge of residual water, recreational activities in the depressions and the leaching of solid waste.

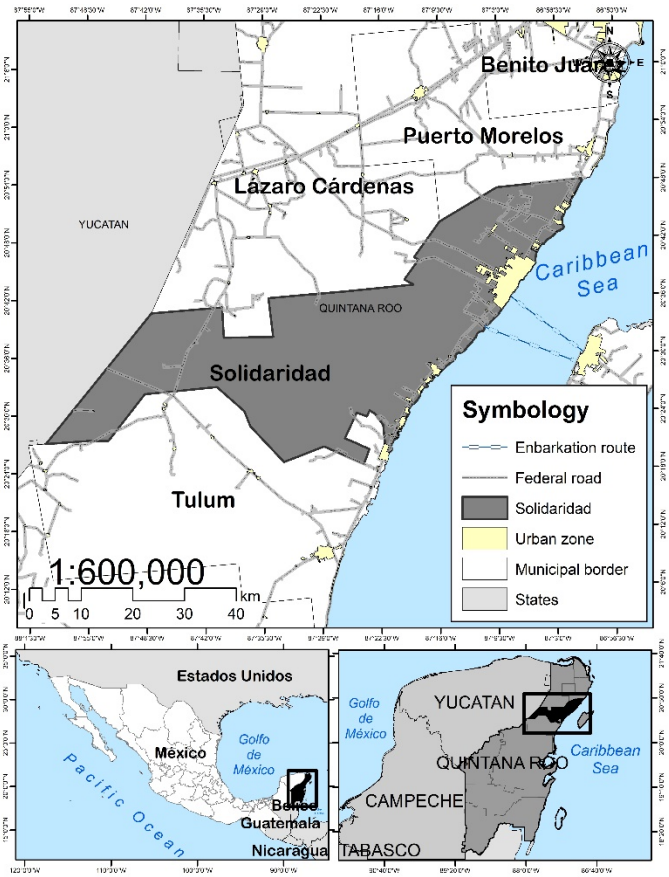

Figure 1. Location of the study area

3.2 Methods and techniques

A sequence of techniques and tools was followed to achieve the objectives and goals of this research (Figure 2). This was performed automatically with the sinkhole-filling method [18, 21, 34-36].

Hydraulic models, altimetry, karst relief, and urban analysis of the karst come from the identification, analysis, and classification of karst depressions with the construction of a Digital Elevation Model (DEM) obtained from two altimetry data sources: (a) LiDAR data mosaic, and (b) Aster GDEM data mosaic, which were combined to produce altimetric data and morphometric base models.

The LiDAR data system available for the Solidaridad region was used [37]. Information was processed in an area of 861.04 km^2. Subsequently, using the LiDAR analysis modules included in the Global Mapper v.18 software [38], the LiDAR mosaic was migrated, and a 3D visualization DEM grid was processed; the contour lines were made equidistant at 0.25 cm, in a range of 0 to 19.5 m (maximum altitude in the northern area of Solidaridad). The process of extracting contour lines from Global Mapper due to a notable improvement in the appearance of the contours allowed the file to be exported in vector format with the elevation, projection, and auxiliary values for 3D modeling; thus, it was possible to produce cartography with a detailed scale of 1:10,000, data resolution of 5 m for the X and Y axes and 0.50 cm for the Z axis [20].

The Aster GDEM V2 [39] is in a grid structure with 30 m resolution and 1 × 1-degree mosaics, available in NASA's EARTHDATA viewer. The data in an area of 1,162.87 km^2 were used. The online data connection and download module included in the Global Mapper were used to obtain the data. Level curves were extracted from the resampled product, with an equidistance of 0.50 cm and a range of altitude 0 to 50 m [40]. The process generated cartography at a scale of 1:20,000 with a data resolution of 30 m for the X and Y axes and 1 m for the Z axis, mainly in areas with little information and relief with low altitude contrast without LiDAR information being available.

10,672 karst depression units were identified, of which 4,498 were recorded in the LiDAR mosaic, and 6,174 units were identified in the Aster GDEM model. Taking a minimum depth of 1 m as a criterion, the maximum heights (scarps) and the minimum elevations (bottoms) were recognized for each depression, which converted the polylines to polygons [8, 22].

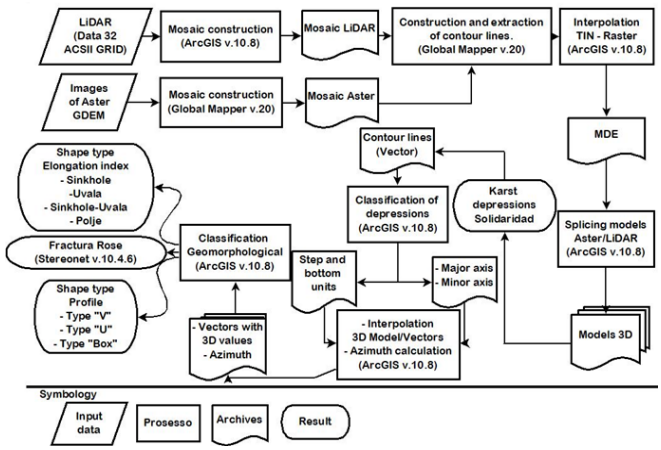

Figure 2. Methodological diagram of techniques and tools

Using ArcGIS v. 10.8 software [41], the karst depressions were identified, and the maximum heights (scarps) and minimum heights (bottoms) of each were determined. Subsequently, using the "Polyline to polygon" tool, the polylines marked on the scarps and scarps were transformed into polygons. Each scarp was assigned a unique ID, maintaining their respective heights in the attribute table [8, 22].

Subsequently, the major and minor axes were drawn semi-automatically in each depression, with the scarp as the limit. For the classification by elongation index, the depression unit

was typified concerning the scarp's width (minor axis) and length (major axis). The index classified less than 1.25 as a sinkhole; those with an index of more than 1.25 but less than 1.75 were those in the transition from sinkholes to uvalas; the uvalas had an index between 1.75 and 2; and finally, all those with an index greater than 2 were classified as poljes [9, 10].

The azimuth of the major axes was obtained considering that each line has measurements that describe its direction and distance; these measurements were useful for describing coordinate geometry. Stereonet v.10.4.6 [42] software was used to calculate the directions and the orientation of the fracture rosette with it.

An interpolation process was used to process the three-dimensional models, which gave a TIN-type file. This represented a surface through an irregular network of triangles generated from the linear interpolation method of the contour lines with the Delaunay triangulation method, which quantifies and models their 3D properties [8]. An interpolation of the polygons was performed with the TIN using the "Interpolate shape" tool, which allowed elevation values to be assigned to the vectors. The interpolation method depends on the type of surface used; in this case, linear interpolation was chosen as the default method for the LAS dataset. This methodology obtains the plane's elevation defined by the triangle containing the XY location of the vector used. A Z-factor of 1 was used, which indicates the factor by which the Z-values will be multiplied. This factor commonly converts linear Z units to match linear XY units. In this study, using a Z-factor of 1 ensured that the elevation values were not altered [24].

The area of each scarp was obtained, and the maximum and minimum elevation values were added to the vectors. Finally, these two values were subtracted to obtain the relative depth of each depression. The scarp polygons were interpolated with the TIN to calculate the volume and area between a polygon of constant surface height [22, 43].

The longitudinal profiles were visualized and interpreted with the "3D Analyst" tool to provide the profile graphs with the later classification of the profile shapes in “V”, “U” and “box”, the depth and gradient of the slopes [8, 21, 22, 24].

4. RESULTS

10,672 units of karst depressions were identified: 2,425 “U”-shaped units, 1,063 “box”-shaped, and 7,184 V-shaped. These depression units were identified from the morphological analysis of topographic profiles for each one. The karst depressions in the form of "V" accounted for 67.3% of the total and were distributed in the eastern part of the study area, “U” shaped depressions corresponded to 22.72% and were distributed mainly along the coastal zone (Figure 3).

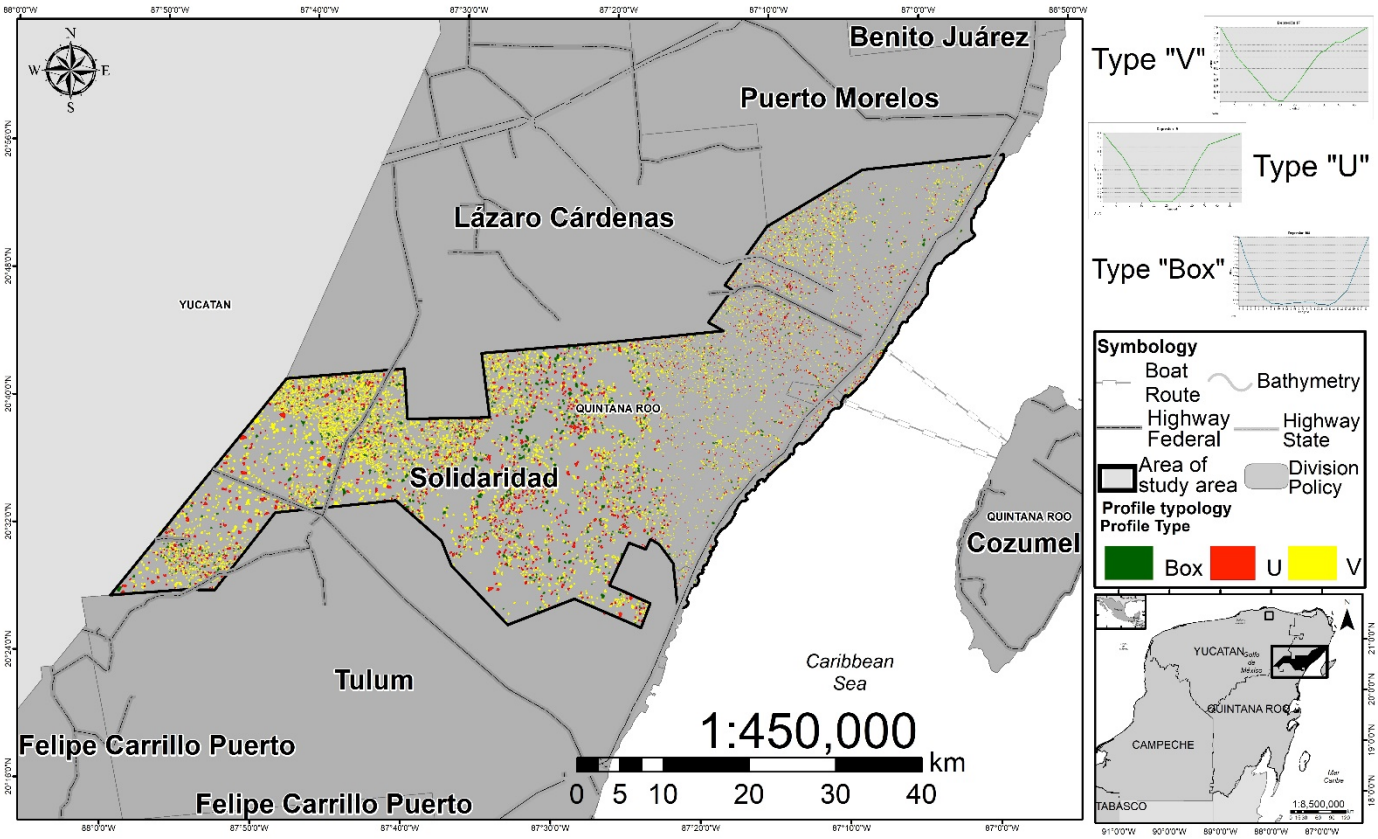

Figure 3. Percentage profile shape distribution

In the graphs in the upper right corner, you can see the shapes of the profiles ("V", "U" and "Box") plotted according to their depth (x-axis) and length (y-axis)

In the profiles, the depressions in the form of "bowls" were those with a greater relative depth compared to the "U" and "V" unit forms, with up to 44.50 m deep in some units and 5 m on average, while the deepest “U” and “V” unit types reached 32.5 m and 24 m, respectively, and 4.6 m and 3.6 m on average. However, the area established by the scarp of the units was higher in the "V" depressions, with up to 300,515 m^2, followed by the "U"-shaped units, with up to 219,966 m^2, and lastly, the bowl-shaped depressions, with scarps of up to 179,621 m^2 surface area.

Sinkholes had an average depth of 4.09 m and maximum and minimum areas of 257,815.2 m^2 and 302.8 m^2, with an

average of 9,376.2 m^2. For sinkholes-uvalas, the maximum depth was 34 m. These units had a relatively larger area than the rest of the forms, with a maximum of 300,515.5 m^2, a minimum of 226.6 m^2, and an average of 10 172 m^2. These same units already formed as uvalas change their features, with a maximum depth of 32 m and average depth of 3.6 m, and the area fluctuating between a maximum of 218,281.8 m^2 and a minimum of 386.49 m^2, with an average of 11,581.2 m^2. The poljes are the formations of the larger area, with a maximum of 237,109.2 m^2 and a minimum of 219.8 m^2, where the depth ranged between 38 m and 1 m, with an average of 3.9 m.

The main orientation of the major axes oscillated between the courses NE 1°SW and NE 9°SW, and a secondary orientation between SE 81°NW and SE 89°NW. Similarly, the sinkholes and sinkholes-uvalas were oriented in the same direction, as this classification represented 42% of all forms. The poljes and uvalas were oriented between NE 41°SW and NE 49°SW. The fracture diagrams and the classification by elongation index over the study area in Figure 4 can be seen together.

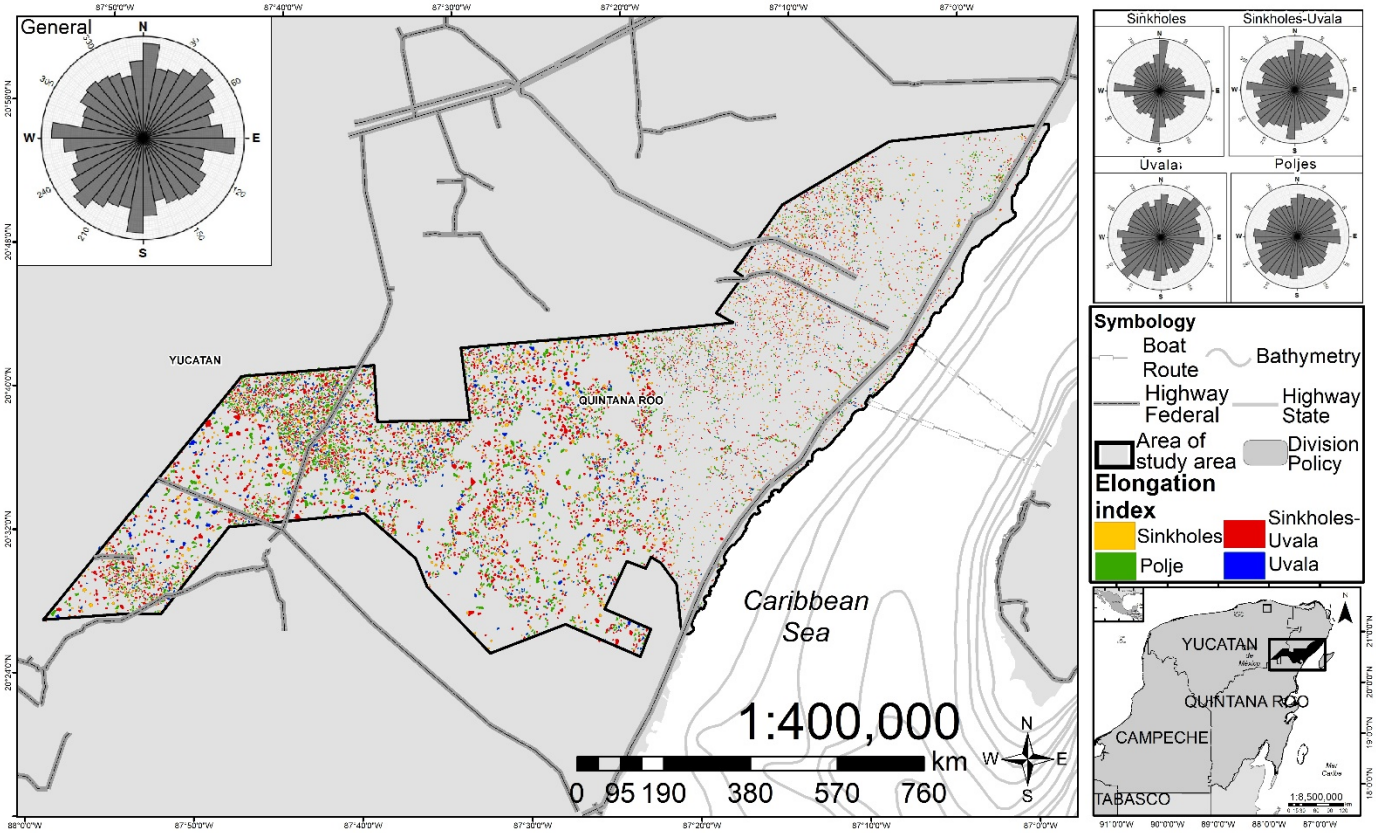

Figure 4. Typological distribution by elongation index, with fracture rosettes grouped by their classification

Finally, Figure 5 shows examples of the 3-dimensional models of the representative units. Their configuration concerning the typology proposed in this study and the complexity of the relief can be seen.

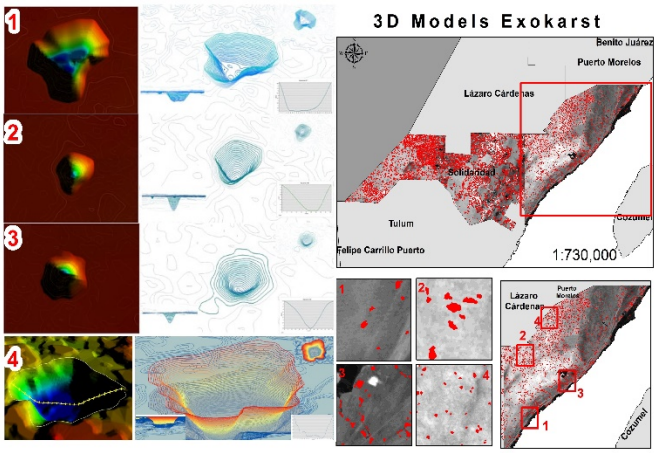

Figure 5. 3D models of representative shapes

5. DISCUSSION

Improved methodologies for detecting and characterizing karst depressions allow for improved information and efficient information and resource management [18].

One of the first contributions to the improvement of these processes was made by Kobal et al. [44], in which they characterized, using a geomorphometric analysis applied to LiDAR technology, the karst depressions of an area characterized by its high tree density for this, they carried out a flow simulation methodology that is fragmented into four phases. In the first phase, the basins were delimited. In the second phase, the cells with the lowest altitude were confined; in the third phase, the recognized karst depressions were divided by grade so that in the fourth phase, the false depressions could be purified, which allowed him to find a correlation between the circularity of the depression with the assigned grade. The maximum depth found was 52m, and the study area had a karst density of 51/km^2. Compared to this study, a karst density of 5/km^2 was found in the whole study area; for LiDAR, it was 9/km^2, and for Aster DEM, it was 3.4/km^2.

On the other hand, Zhu et al. [36] conducted a methodology based mainly on sinkhole backfilling, which consists of delineating the watershed, estimating the flow direction, locating the focused flow, and zonally backfilling. It was found to have a reliability of 80% to 93%, depending on the field data for comparison. This is compared to other methodologies, such as Zhu and Pierskalla [18], which conducted an automated study with a random forest method to extract sinkholes in a karst region in central Kentucky automatically and obtained an 89% accuracy with LiDAR with a resolution of 1 m^2. Compared to the previously mentioned method of filling sinkholes but passing the resulting information to polygons, this was done through the compactness index to extract the least irregular shape possible, reaching an accuracy of 77%. Čonč et al. [34], with their analysis, found the same limitation in assigning the edge of karst depressions on sloping surfaces. This does not allow for finding the real shape of the karst depression, resulting in reduced accuracy.

In this study, the morphology of the shapes given by the generated contour lines was maintained, and the corresponding contour lines were extracted so as not to affect the modeled shape of the depression. Wall et al. [35], with inventories of karst depressions in the area, obtained 85% with a resolution of $10m^2$ and a resolution of $1m^2$, reaching up to 93% accuracy. This method was also used by Telbisz et al. [21], who made a new 3D classification index using the sinkhole filling method, but with adjustments in the flow direction process, to level the slope of the depressions and counter-arrest the limitation found by Čonč et al. [34].

The use of mapping from new and updated sources allows a better characterization of karst terrain; this study focuses on the resolution and model coupling of source data. LiDAR data has a data resolution of 5m for the X, Y, and 0.50cm for the Z axis; the Aster GDEM data has a resolution of 30m for the X, Y, and 1m for the Z axis. However, the coupling of models complements the inventories of those territories where LiDAR data does not exist in the Yucatan peninsula.

The studies generated by Fragoso-Servón et al. [10], Fragoso-Servón et al. [28], Pereira-Corona et al. [29] and Paredes et al. [19] in Yucatan, which used models with a minimum resolution of 15m, generating hypsometric contour lines at a scale of 1:50 000, have a limiting spatial resolution for the characterization of specific areas of the peninsula. This study takes advantage of the indices generated by Frausto-Martínez et al. [9], the methodology of Colín-Olivares et al. [22] for automated calculations, and the study by Frausto-Martínez et al. [8] with the typological classification by profile type since, in addition to generating models from the interpolation of the major axis with the DEM, morphometric calculations of the relief were carried out for its classification, automating and improving the obtaining of morphometric indices with the interpolation of the altitudinal values of the DEM. This means that in a single application, the calculation of the marked units was automated in a single execution of the triangulation of the shapefile with the scarp polygons, obtaining the total volume and the area of each karst depression from the scarp.

Similarly, Telbisz et al. [21] used LiDAR-based Digital Terrain Models (DTM) to investigate small-scale geomorphological features, such as dolines in karst terrain. They have analyzed the size distribution of morphometric parameters of dolines and how to characterize their volume. He compared the LiDAR data of dolines with topographic maps and thus analyzed the relationships between doline parameters, topography, and geological features. The results showed that the LiDAR-based doline density is 25% higher than topographic maps. LiDAR-based dolines are slightly larger and less rounded. The thickness of dolines varies according to slope and lithology. From a new parameter, the DTM-based doline volume is described, which indicates whether the shape of the doline is more like a cylinder, a bowl, a cone, or a funnel.

"V" and "U" depressions are more abundant in the study area, with a predominance of the "V", due to karst depressions being influenced by meteoric diagenesis processes, intensified by horizontal hydraulics, exogenetic sedimentation, and cementation processes along units parallel to paleo-dune systems and coastal lithological boundaries [43-47]. “V” type karst depressions are associated with lithological systems with a high level of porosity, which are filled at the time of collapse and whose morphology indicates that the karst processes are recent [47-49]. They are also known as “Aguada” and serve as a natural pond with a lot of organic activity [49, 50]. The karst formations in the bowl type of depression are an indicator of contact with the water table due to the dissolution of the rock before the roof collapsed [21, 47, 49, 51]. These forms are also classified with their regional name as “cenote” [9, 25, 30].

Sinkholes are dissolution units and indicators of contact with the water table and the result of meteorological-geological action [11, 25, 50]. With the gradual passage of time, these processes can give rise to formations with a larger area and/or dissolution axis of the sinkholes-uvalas and/or uvala type. Uvalas with extraordinary flooding are indicators of greater solubility in the rock and, therefore, living processes of karstification [16, 23, 43]. Poljes are units of organic matter accumulation processes because they have good drainage and a high rate of evapotranspiration [52].

The fractures in the rocks control the positioning of the karstic forms due to the greater intensity of rock dissolution that occurs in them [19]. The Yucatan Peninsula is a limestone platform with a neotectonic activity that favors forming a system of faults oriented mainly to the N-S and NE-SW [10, 19].

These combined dissolution processes, both meteorological and geological, are responsible for the formation of sinkholes [48, 53]. Over time, these processes can give rise to formations of greater area and/or axis of dissolution, giving rise to uvula-sinkholes and/or uvalas [11, 43]. These processes recreate patterns that can be associated at the surface with the behavior of groundwater and/or surface water layers [33, 49, 51]. This behavior is related to the number of cave systems explored in this region, considering that 47% of the units belong to this type of form [43, 47]. The poljes are units where organic matter accumulation processes predominate, as they have good drainage and a high rate of evapotranspiration [11, 14, 54].

6. CONCLUSION

(1) The characterization of the northeast area of the Yucatan Peninsula allows the processes shaping the karst relief to be understood, as this land is sensitive to changes and environmental modifications. Geomorphological characterization can be performed with the applied morphometric indices.

(2) Using topographic profiles and classification by the

elongation index makes it possible to understand the evolution of depressions, which are also produced by vertical dissolution. In addition, they also allow the degree of infiltration associated with the materials and the complex drainage system of this type of relief to be understood, highlighting indicators of area and volume.

(3) The orientation of the major axes of the depressions allows us to propose a structural genesis for the units and processes associated with modeling the karst landscape.

(4) Identifying karstic depressions provides primary information for fulfilling inventories for managing territories at the municipal level. It also provides key information for applying management regulations for karst areas in the northeast of the Yucatan Peninsula.

ACKNOWLEDGMENT

This work is supported by the CONAHCYT (For its acronym in Spanish: Consejo Nacional de Humanidades, Ciencia y Tecnología in México) and Postgraduate Program of Marine and Coastal Science and the Sustainable Development Division of the Universidad Autónoma del Estado de Quintana Roo (Grant No.: 1201924).

REFERENCES

[1] Waele, J.D., Plan, L., Audra, P. (2009). Recent developments in surface and subsurface karst geomorphology: An introduction. Geomorphology, 106(1-2): 1-8. https://doi.org/10.1016/j.geomorph.2008.09.023

[2] Veni, G. (1999). A geomorphological strategy for conducting environmental impact assessments in karst areas. Geomorphology, 31(1-4), 151-180. https://doi.org/10.1016/S0169-555X(99)00077-X

[3] Macedo, F.R., Souza, M.L.D. (2018). Elaboração de perfil topográfico utilizando softwares vetoriais. Revista de Geografia, Meio Ambiente e Ensino, 9(1): 83-94.

[4] Morais, F., Soriano, M.A. (2017). Análisis morfométrico de dolinas y parámetros geofísicos aplicados al estudio de los flujos de agua subterránea en la Cuenca Del Ebro, Zaragoza, España. Geosciences = Geociências, 36(2): 221-232. https://doi.org/10.5016/geociencias.v36i2.10892

[5] Williams, P.W. (1972). Morphometric Analysis of Polygonal Karst in New Guinea. GSA Bulletin, 83(3): 761-796. https://doi.org/10.1130/0016-7606(1972)83[761:MAOPKI]2.0.CO;2

[6] Ibarra-Marigal, S.M., Hernández-Montero, Y.N., Nahuat-Sansores, J.R., Rejón-Parra, D.G., Sánchez-Quijano, M.Á., Mena-Rivero, R., Torrescano-Valle, N., Arellano-Guillermo, A., Romero-Martínez, Á.I. (2022). Diseño urbano sensible al agua para la zona kárstica de Bacalar, Quintana Roo, México. Ecosistemas y Recursos Agropecuarios, 9(2). https://doi.org/10.19136/era.a9n2.3236

[7] Madrigal, S.M.I., Gracia, M.A., Schmook, B., Arana, H.A.H. (2020). Ordenamiento territorial, agua subterránea y participación sociopolítica en Bacalar, Quintana Roo, México. Sociedad y Ambiente, 22: 265-292. https://doi.org/10.31840/sya.vi22.2112

[8] Frausto-Martínez, O., Rodríguez-Castillo, J.F., Colín-Olivares, O. (2021). Morfometría de depresiones kársticas a escala detallada: El Cedral, Cozumel – México. Tropical and Subtropical Agroecosystems, 24(1). https://doi.org/10.56369/tsaes.3657

[9] Frausto-Martínez, O., Colín-Olivares, O., Rodríguez-Castillo, F. (2021). Karst en la ciudad: planificación del espacio urbanístico de la ciudad de Cozumel, México. Tropical and Subtropical Agroecosystems, 24(1). https://doi.org/10.56369/tsaes.3588

[10] Fragoso-Servón, P., Bautista, F., Frausto, O., Pereira, A. (2014). Caracterización de las depresiones kársticas (forma, tamaño y densidad) a escala 1: 50,000 y sus tipos de inundación en el Estado de Quintana Roo, México. Revista Mexicana de Ciencias Geológicas, 31(1), 127-137.

[11] Ford, D.C., Williams, P.W. (1989). Karst Geomorphology and Hydrology. London: Unwin Hyman.

[12] Moreno-Gómez, M., Pacheco, J., Liedl, R., & Stefan, C. (2018). Evaluating the applicability of European karst vulnerability assessment methods to the Yucatan karst, Mexico. Environmental Earth Sciences, 77(19): 682. https://doi.org/10.1007/s12665-018-7869-5

[13] Back, W. (1995). Water management by early people in the Yucatan, Mexico. Environmental Geology, 25(4): 239-242. https://doi.org/10.1007/BF00766752

[14] Bauer-Gottwein, P., Gondwe, B.R.N., Charvet, G., Marín, L.E., Rebolledo-Vieyra, M., Merediz-Alonso, G. (2011). Review: The Yucatán Peninsula karst aquifer, Mexico. Hydrogeology Journal, 19(3): 507-524. https://doi.org/10.1007/s10040-010-0699-5

[15] Lebedeva, E.V, Mikhalev, D.V, Nekrasova, L.A. (2017). Evolutionary stages of the karst-anthropogenic system of the Yucatán Peninsula. Geography and Natural Resources, 38(3): 303-311. https://doi.org/10.1134/S187537281703012X

[16] Lace, M.J., Mylroie, J.E. (2013). Coastal cave and karst resource management. In: Coastal Karst Landforms, pp. 127-143. https://doi.org/10.1007/978-94-007-5016-6_6

[17] Siart, C., Bubenzer, O., Eitel, B. (2009). Combining digital elevation data (SRTM/ASTER), high resolution satellite imagery (Quickbird) and GIS for geomorphological mapping: A multi-component case study on Mediterranean karst in Central Crete. Geomorphology, 112(1-2), 106-121. https://doi.org/10.1016/j.geomorph.2009.05.010

[18] Zhu, J., Pierskalla, W.P. (2016). Applying a weighted random forests method to extract karst sinkholes from LiDAR data. Journal of Hydrology, 533: 343-352. https://doi.org/10.1016/j.jhydrol.2015.12.012

[19] Paredes, C., Matos, H., De la Vega, R., Pardo, E. (2019). Reconocimiento semiautomático de depresiones kársticas mediante análisis de agregados en sus distribuciones morfométricas. Aplicación al karst del Estado de Yucatán, México. Revista Mexicana de Ciencias Geológicas, 36(2): 270-288. https://doi.org/10.22201/cgeo.20072902e.2019.2.1017

[20] Frausto-Martínez, O., Zapi-Salazar, N.A., Colin-Olivares, O. (2018). Identification of karst forms using LiDAR technology: Cozumel Island, Mexico. In: Trends in Geomatics-An Earth Science Perspective. https://doi.org/10.5772/intechopen.79196

[21] Telbisz, T., Mari, L., Székely, B. (2024). LiDAR-Based Morphometry of Dolines in Aggtelek Karst (Hungary) and Slovak Karst (Slovakia). Remote Sensing, 16(5): 737.

https://doi.org/10.3390/rs16050737
[22] Colín-Olivares, O., Frausto-Martínez, O., Rodríguez-Castillo, J.F. (2019). Cálculo automatizado de la profundidad de depresiones kársticas a escala detallada. Conocimientos y Saberes Sobre el Karst de México, pp. 55-77.
[23] Fuchs, M., Reinartz, H., Torizin, J., Balzer, D., Kuhn, D., Schüßler, N., Hahne, K., Nix, T., Gunkel, C. (2024). Mapping karst depressions and sinkholes in anthropogenically influenced areas. Research Square. https://doi.org/10.21203/rs.3.rs-3869389/v1
[24] Uhu-Yam, W.D., Frausto-Martínez, O., Rodríguez-Castillo, J.F., Colín-Olivares, O. (2022). Factores para desarrollar un índice de vulnerabilidad a la contaminación en acuíferos kársticos costeros urbanizados. Ecosistemas y Recursos Agropecuarios, 9(3). https://doi.org/10.19136/era.a9n3.3220
[25] Frausto-Martínez, O., Ihl, T. (2008). Mapas de formas exokársticas del norte de Quintana Roo a escala 1:50000. In: Estudio geohidrológico del norte de Quintana Roo, México, pp. 45-58.
[26] Ihl, T., Martínez, O.F., López, J.R., Giese, S., Goldacker, S., Zúñiga, F.B., Verdinelli, G.B. (2008). Identification of geodisasters in the state of Yucatan, Mexico. Neues Jahrbuch Für Geologie Und Paläontologie-Abhandlungen, 246(3): 299-311. https://doi.org/10.1127/0077-7749/2007/0246-0299
[27] Lindsey, B.D., Katz, B.G., Berndt, M.P., Ardis, A.F., Skach, K.A. (2010). Relations between sinkhole density and anthropogenic contaminants in selected carbonate aquifers in the eastern United States. Environmental Earth Sciences, 60(5): 1073-1090. https://doi.org/10.1007/s12665-009-0252-9
[28] Fragoso-Servón, P., Bautista, F., Pereira, A., Frausto, O. (2016). Distribución de Suelos en ambientes tectokársticos en la porción este de la Península de Yucatán, México. GEOS, 36(2).
[29] Pereira-Corona, A., Fragoso-Servón, P., Frausto, O. (2017). Suelos, agua, inundaciones y cambio climático en zonas de karst: El caso de Quintana Roo, México. GEOS, 36(2): 275-290. https://ugm.org.mx/publicaciones/geos/pdf/geos16-2/suelos-36-2.pdf.
[30] Ferreira, C.F., Uagoda, R.E.S. (2019). Tipologias do carste e classificações de dolinas: Uma revisão. Caminhos de Geografia, 20(70): 519-537. https://doi.org/10.14393/RCG207044169
[31] Rahimi, M., Alexander, C. (2013). Locating Sinkholes in LiDAR Coverage of a Glacio-Fluvial Karst, Winona County, MN. In Full Proceedings of the Thirteenth Multidisciplinary Conference on Sinkholes and the Engineering and Environmental Impacts of Karst, pp. 469-480. https://doi.org/10.5038/9780979542275.1158
[32] Miao, X., Qiu, X., Wu, S.S., Luo, J., Gouzie, D.R., Xie, H.J, (2013). Developing efficient procedures for automated sinkhole extraction from lidar DEMs. Photogrammetric Engineering & Remote Sensing, 79(6): 545-554. https://doi.org/10.14358/PERS.79.6.545
[33] Lei, H.Q., Li, D., Jiang, H. (2023). Enhancement of sonar detection in karst caves through advanced target location and image fusion algorithms. Traitement Du Signal, 40(4): 1593-1660. https://doi.org/10.18280/ts.400427
[34] Čonč, Š., Oliveira, T., Portas, R., Černe, R., Breg Valjavec, M., Krofel, M. (2022). Dolines and cats: Remote detection of karst depressions and their application to study wild felid ecology. Remote Sensing, 14(3): 656. https://doi.org/10.3390/rs14030656
[35] Wall, J., Bohnenstiehl, D.R., Wegmann, K.W., Levine, N.S. (2017). Morphometric comparisons between automated and manual karst depression inventories in Apalachicola National Forest, Florida, and Mammoth Cave National Park, Kentucky, USA. Natural Hazards, 85(2): 729-749. https://doi.org/10.1007/s11069-016-2600-x
[36] Zhu, J., Taylor, T.P., Currens, J.C., Crawford, M.M. (2014). Improved karst sinkhole mapping in Kentucky using lidar techniques: A pilot study in Floyds. Journal of Cave and Karst Studies, 76(3): 207-216. https://doi.org/10.4311/2013ES0135
[37] INEGI. (2023). Datos del terreno LiDAR. Instituto Nacional de Geografía y Estadística. https://www.inegi.org.mx/app/mapas/?tg=1015, accessed on Aug. 3, 2024.
[38] Global Mapper. (2023). Global Mapper v.18. https://www.bluemarblegeo.com/global-mapper/, accessed on Aug. 3, 2024.
[39] ASTER. (2023). ASTER global digital elevation map announcement. https://asterweb.jpl.nasa.gov/gdem.asp, accessed on Aug. 3, 2024.
[40] Schmitter-Soto, J.J., Comín, F.A., Escobar-Briones, E., Herrera-Silveira, J., Alcocer, J., Suárez-Morales, E., Elías-Gutiérrez, M., Díaz-Arce, V., Marín, L.E., Steinich, B. (2002). Hydrogeochemical and biological characteristics of cenotes in the Yucatan Peninsula (SE Mexico). Hydrobiologia, 467(1): 215-228. https://doi.org/10.1023/A:1014923217206
[41] ArcGIS. (2023). ArcGIS v.10.8. https://desktop.arcgis.com/es/arcmap/latest/get-started/installation-guide/installing-on-your-computer.html, accessed on Aug. 3, 2024.
[42] Stereonet. (2023). Stereonet v.10.4.6. https://www.rickallmendinger.net/stereonet, accessed on Aug. 3, 2024.
[43] Bradshaw, K.K., Ray, T.S. (2020). Modelling the positive feedback mechanism of a karst aquifer using surface reconstruction. International Journal of Computational Methods and Experimental Measurements, 8(4): 367-386. https://doi.org/10.2495/CMEM-V8-N4-367-386
[44] Kobal, M., Bertoncelj, I., Pirotti, F., Kutnar, L. (2014). Lidar processing for defining sinkhole characteristics under dense forest cover: A case study in the Dinaric Mountains. The International Archives of the Photogrammetry, Remote Sensing and Spatial Information Sciences, 40: 113–118. https://doi.org/10.5194/isprsarchives-XL-7-113-2014
[45] Fleury, P., Bakalowicz, M., de Marsily, G. (2007). Submarine springs and coastal karst aquifers: A review. Journal of Hydrology, 339(1-2): 79-92. https://doi.org/10.1016/j.jhydrol.2007.03.009
[46] Kambesis, P.N., Coke, J.G. (2013). Overview of the controls on eogenetic cave and karst development in Quintana Roo, Mexico. In: Coastal Karst Landforms, pp. 347-373. https://doi.org/10.1007/978-94-007-5016-6_16
[47] Cao, X., Tang, H., Liu, Z., Li, H. (2020). Dissolution features of karst foundations at different depth sections. International Journal of Design & Nature and Ecodynamics, 15(2): 145-153.

https://doi.org/10.18280/ijdne.150202
[48] Zhang, B., Xie, Y., Li, H., Liu, B. (2020). Distribution pattern of rock face dissolution degree with depth in building foundation in the karst terrain of Southwest China. International Journal of Design & Nature and Ecodynamics, 15(2): 261-268. https://doi.org/10.18280/ijdne.150217
[49] Wahid, A., Sunaryo, Susilo, A., Wiyono. (2022). Identification of karstification zoning and aquifer channels in karst basin at Sendang Biru beach, Malang-Indonesia: A case study. International Journal of Design & Nature and Ecodynamics, 17(3): 391-400. https://doi.org/10.18280/ijdne.170309
[50] Gaona-Vizcayno, S., Gordillo-de Anda, T., Villasuso-Pino, M. (1980). Cenotes, karst característico: Mecanismos de formación. Revista Mexicana de Ciencias Geológicas, 4(1): 32-36.
[51] Carrión-Mero, P., Olaya, P., Sanango-Ochoa, L., Cano-Alvarado, F., Bravo-Montero, Lady, Solórzano, J., Morante-Carballo, F. (2023). Hydrogeological characterization of a coastal area for the groundwater exploitation. Hondo river micro-watershed, Santa Elena-Ecuador. International Journal of Sustainable Development and Planning, 18(2): 401-410. https://doi.org/10.18280/ijsdp.180208
[52] Schoeneberger, P.J., Wysocki, D.A. (2005). Hydrology of soils and deep regolith: a nexus between soil geography, ecosystems and land management. Geoderma, 126(1-2): 117-128. https://doi.org/10.1016/j.geoderma.2004.11.010
[53] Gil-Márquez, J.M., Durán-Valsero, J.J., Andreo, B. (2024). Introductory editorial to the topical collection: hydrogeological and geomorphological advances in karst and caves research. Environmental Earth Sciences, 83(2): 54. https://doi.org/10.1007/s12665-023-11382-4
[54] Vuilleumier, C., Borghi, A., Renard, P., Ottowitz, D., Schiller, A., Supper, R., Cornaton, F. (2013). A method for the stochastic modeling of karstic systems accounting for geophysical data: An example of application in the region of Tulum, Yucatan Peninsula (Mexico). Hydrogeology Journal, 21(3): 529-544. https://doi.org/10.1007/s10040-012-0944-1